

Impact of Femtosecond Laser Treatment Accompanied with Anodization of Titanium Alloy on Fibroblast Cell Growth

Shaukat Ali Lone, Martina Muck, Peter Fosodeder, Cezarina Cela Mardare, Camilo Florian, Agnes Weth, Jörg Krüger, Clemens Steinwender, Werner Baumgartner, Jörn Bonse, Johannes Heitz, and Achim Walter Hassel*

Herein, Ti6Al4V alloy is surface modified by femtosecond laser ablation. The microstructure image obtained by secondary electron microscopy reveals a combination of micrometer spikes or cones superimposed by nanoripples (laser-induced periodic surface structures). To make the surface hydrophilic, anodization is performed resulting in further smoothness of microstructure and a final thickness of 35 ± 4 nm is estimated for oxide produced after anodization at 10 V (scan rate = 0.1 V s^{-1}) versus standard hydrogen electrode. The obtained electrochemically active surface area (ECSA) is approximately 8 times larger compared with flat mirror polished Ti6Al4V surface. Combined chemical analysis by Pourbaix diagram and X-ray photoelectron spectroscopy (XPS) analyses reveal that titanium and aluminum are passivating into TiO_2 and Al_2O_3 , but the dissolution of aluminum in the form of solvated ion is inevitable. Finally, cell seeding experiments on anodized and laser-treated titanium alloy samples show that the growth of murine fibroblast cells is significantly suppressed due to unique surface texture of the laser-treated and anodized titanium alloy sample.

body-centered cubic structure (β -phase) above 882.5°C .^[1] However, the β -phase can be stabilized at room temperature by incorporating certain alloying elements. Mainly aluminum is used to stabilize, i.e., retain the α -phase and elements such as V, Cr, Cu, Si, Nb, or Fe are used to stabilize the β -phase.^[1–4] It was reported that α -phase titanium alloys have superior corrosion resistance and the β -phase ones exhibit relatively better low-temperature formability, lower or comparable elastic modulus with natural bone material resulting in a better wear resistance.^[5]

The Ti6Al4V alloy ($\alpha + \beta$) has been extensively used in biomedical implants,^[6] i.e., cardiac heart pacemakers^[7] and bone fixer implants, due to its excellent biocorrosion resistance, biocompatibility, durability, and mechanical properties.^[8]


1. Introduction

Pure titanium exhibits at room temperature a hexagonal closed packed structure (α -phase), which thermally transforms to

Nevertheless, the dissolution of vanadium and aluminum (that are considered as toxic materials) into the body is a matter of concern for future usage.^[9] The ionic dissolution is dependent upon the corrosion rate and it is a well-known fact that the

S. A. Lone, Prof. A. W. Hassel
Christian Doppler Laboratory for Combinatorial Oxide Chemistry
Institute of Chemical Technology of Inorganic Materials (TIM)
Johannes Kepler University Linz
Altenberger Str. 69, 4040 Linz, Austria
E-mail: achimwalter.hassel@jku.at

S. A. Lone, Dr. C. C. Mardare, Prof. A. W. Hassel
Institute of Chemical Technology of Inorganic Materials (TIM)
Johannes Kepler University Linz
Altenberger Str. 69, 4040 Linz, Austria

 The ORCID identification number(s) for the author(s) of this article can be found under <https://doi.org/10.1002/pssa.201900838>.

© 2020 The Authors. Published by WILEY-VCH Verlag GmbH & Co. KGaA, Weinheim. This is an open access article under the terms of the Creative Commons Attribution-NonCommercial-NoDerivs License, which permits use and distribution in any medium, provided the original work is properly cited, the use is non-commercial and no modifications or adaptations are made.

DOI: 10.1002/pssa.201900838

M. Muck, P. Fosodeder, Prof. J. Heitz
Institute of Applied Physics
Johannes Kepler University Linz
Altenberger Str. 69, 4040 Linz, Austria

Dr. C. Florian, Dr. J. Krüger, Dr. J. Bonse
Bundesanstalt für Materialforschung und -prüfung (BAM)
Unter den Eichen 87, 12205 Berlin, Germany

A. Weth, Prof. W. Baumgartner
Institute of Biomedical Mechatronics
Johannes Kepler University Linz
Altenberger Str. 69, 4040 Linz, Austria

Dr. C. Steinwender
Department of Cardiology
Kepler University Hospital Linz
Krankenhausstraße 9, 4020 Linz, Austria

corrosion rate of valve metals can be significantly decreased by anodization.^[10–13]

Cellular growth is considered to be initiated by an adsorbed layer of specific proteins from the body fluid onto the implant surface.^[14] Cohesion or repulsion of these proteins are mainly influenced by the ion or charge distribution,^[15] wettability,^[16] and morphology^[17] of the implant surface. Depending upon the location of the implant inside the body, it is important to know how these implants are interacting with the cells, e.g., novel miniaturized cardiac heart pacemakers that are directly implanted in the right ventricle of the heart ideally should not be fully overgrown by the scar tissue as they may have to be removed after several years.^[7]

To address these issues, several surface and chemical treatment procedures have been undertaken in the past, i.e., sand blasting,^[18] electrochemical polishing,^[19] ion implantation,^[20] and physical and chemical vapor deposition.^[21] The femtosecond (fs) laser ablation is a unique surface treatment process through which various morphologies can be induced on the irradiated surface by changing laser processing parameters, i.e., energy per unit area, effective number of pulses per unit area, and scanning speed^[22] without incorporating impurities. Müller et al. explained that ultrashort laser scan processing with Gaussian beam distribution on different materials can result in hierarchical surface morphologies, which exhibit superhydrophobicity.^[23] Moreover, the latter structure has also been reported to control the cell growth.^[24]

Anodization is an electrochemical process by means of which a thick oxide layer is grown on the valve metal surface, i.e., Ti, Ta, and Nb.^[25,26] This technique can not only introduce some chemical changes to the Ti–O bond,^[8] which in turn influences the cell growth, but also can affect the wettability of the surface.^[27] Increased wetting of the surface is significantly recommended for the proper contact of the body fluid (e.g., blood) to the implant surface.

In this work, we study the combined effect of fs laser treatment and anodization on the microstructural, chemical, and fibroblast cell growth properties of Ti6Al4V alloy.

2. Experimental Section

A rod of 25 mm diameter of grade 5 Ti6Al4V was purchased from Schumacher Titan GmbH, Germany. The rod was cut in the form of circular disks having a thickness of 8 ± 0.3 mm and subsequently mechanically polished resulting in a mirror-like surface finish. To study the oxide properties, a 1 mm thin sheet medical grade Ti6Al4V (ZAPP Metals GmbH, Germany) was also used for selected experiments. The energy-dispersive X-ray spectrometer (EDX) analysis of the sheet Ti6Al4V alloy revealed a composition of 90 wt% Ti, 5.7 wt% Al, and 4.3 wt% V.

A Ti:sapphire fs laser amplifier system was utilized to generate a Gaussian-shaped spatial beam profile in the laser beam focus with a $\frac{1}{e^2}$ radius of $W_0 = 38.2$ μm . An area of 3.5×3.5 mm^2 was laser processed with linearly polarized laser pulses ($\tau = 30$ fs, $E = 70$ μJ , pulse repetition frequency = 1 kHz) at five different spots on circular disk samples. The peak fluence in front of the sample surface was calculated by the formula ($\frac{2E}{\pi W_0^2} = 3$ J cm^{-2}).

By considering the laser scan velocity ($v_x = 0.191$ $\mu\text{m s}^{-1}$) and the diameter D of the laser spot ($2W_0 = 76.4$ μm), the effective number of laser pulses at a focused laser spot was also evaluated ($N_{\text{eff}} = \frac{Df}{v_x} = 400$). After the fs laser treatment of the Ti6Al4V alloy surface, the samples were ultrasonically cleaned in acetone bath.

All electrochemical measurements were done using a flow-type scanning droplet cell microscope (FT-SDCM).^[28] As shown in **Figure 1a**, the electrochemical cell consisted of a gold counter electrode, Au/Hg/Hg₂SO₄ in 0.1 M H₂SO₄ reference electrode, and fs laser-treated or mirror-like finished Ti6Al4V samples as working electrode. An acidic electrolyte (0.1 M H₂SO₄) was used for anodization. The electrolyte was pumped via a peristaltic pump by means of a V-shaped channel into the electrochemical cell. The intersection point of this V-shaped channel contains an opening encircled with an in-house developed sealing through which the electrolyte was exposed to the working electrode. The exposed area (0.2835 cm^2) of the SDCM was measured

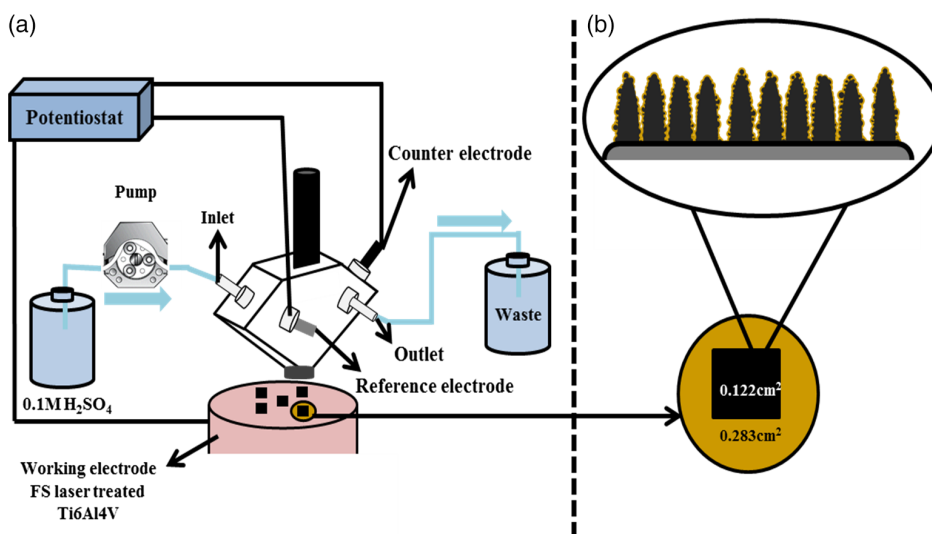


Figure 1. a) Schematic diagram of the electrochemical setup containing three-electrode FT-SDCM electrically connected to a potentiostat and controlled supply of 0.1 M H₂SO₄ electrolyte via a peristaltic pump. b) Exemplary anodized layer of oxide grown on the surface of hierarchical spike-like structure induced by fs laser ablation.

carefully after analyzing the anodized spot under an optical microscope.^[29] Several exemplary anodizing experiments were done on pure Ti with different forces applied between the working electrode surface and the outer rim of the SDCM, as well as with various pump rotation speed to avoid gas accumulation and to achieve best colored anodized spots. After a careful examination, a rotation speed of 500 rpm and a force of 4 N were selected for further experiments. To study the oxide properties of the polished flat surface and fs laser-treated Ti6Al4V sample, a maximum potential of 7 V was applied with a 1 V stepwise increment in voltage at a scan rate of 0.1 V s^{-1} . Finally, for the fibroblast cell experiment, the fs laser-treated sample was anodized at 10 V with the scan rate of 0.1 V s^{-1} . The scan rate is important as it decides on the duration of the experiment and strongly influences the trap density in the oxide.^[30,31] This will have a direct influence on the ionic/electronic conductivity of the resulting oxide film which in turn influences the reaction at the passive titanium film such as oxygen evolution or protein denaturation.^[13] After anodization, the samples were washed with acetone, cleaned with deionized (DI) water, and blown by compressed air to remove any solvent or impurities. All potentials were reported versus standard hydrogen electrode (SHE).

Scanning electron microscopy (SEM) was used for surface morphological characterization (Zeiss 1540XB). The elemental quantification of the bulk alloy was achieved using an in-built EDX from INCA X-Sight Oxford Instruments operating with an accelerating voltage of 20 kV. Surface elemental quantification was also conducted by X-ray photoelectron spectroscopy (XPS; Thermo Scientific, Theta probe). A spot size of $400 \mu\text{m}$ diameter was used for the analysis. For each wide spectrum survey, a step size of 1 eV and a dwell time of 0.1 s were applied with seven sweeps for each energy scan. For high-resolution scans, a step size of 0.05 eV and a dwell time of 0.1 s were used for a particular energy region with ten sweeps in total.

For cell adhesion testing, murine fibroblast cells from the cell line LTK (ECACC 85011432, UK) were used. The fibroblast cells

were grown in Dulbecco's Modified Eagle Medium (DMEM, Lactan, Graz, Austria) to which 2 mM glutamine (Sigma) and 10% fetal calf serum (FCS, Biochrom, Berlin, Germany) were added. Furthermore, 50 U mL^{-1} penicillin and streptomycin (Serva, Heidelberg, Germany) were also added. The cell growth took place at 37°C in H_2O -saturated atmosphere containing 5% CO_2 . Once a week, the cells were split at a ratio of 1:10. The laser structured Ti6Al4V alloy samples were placed in a petri dish containing the respective murine fibroblast cell for 1 week to promote and observe the cell growth and adherence.

To view the morphology and murine fibroblast cell attachment on laser-treated Ti6Al4V samples, SEM (Philips SEM 525, Germany) images were obtained. Before the SEM analysis, the cells were initially fixed overnight with 6% glutaraldehyde (GA; Merck, Darmstadt, Germany) in phosphate-buffered saline (PBS) and subsequently dehydrated with the help of ascending ethanol series (30%, 40%, 50%, 70%, 80%, 90%, 96%, $3 \times 100\%$) for 30 min each. The samples were repeatedly transferred 3 times into 100% hexamethyl-disilazane (HMDS; Merck). After the overnight evaporation of HMDS, samples were sputter-coated with gold and analyzed under SEM.

The Pourbaix diagrams for titanium, aluminum, and vanadium were computed at 298 K, atmospheric pressure, and at an ionic concentration of 10^{-6} M dissolved species in 0.1 M H_2SO_4 using Medusa software.^[32] The murine fibroblast cell experiments were done with the similar procedure as explained in a previous work by Heitz et al.^[33]

3. Results and Discussion

Figure 2a–d shows the SEM images of the fs laser-treated surface taken at four different magnifications under a tilt angle of 0° (Figure 2a) and 60° (Figure 2b–d). Blue arrows indicate the laser polarization orientation. Further magnified images (Figure 2b,c) demonstrate laser-induced cone or spike-like structure. These

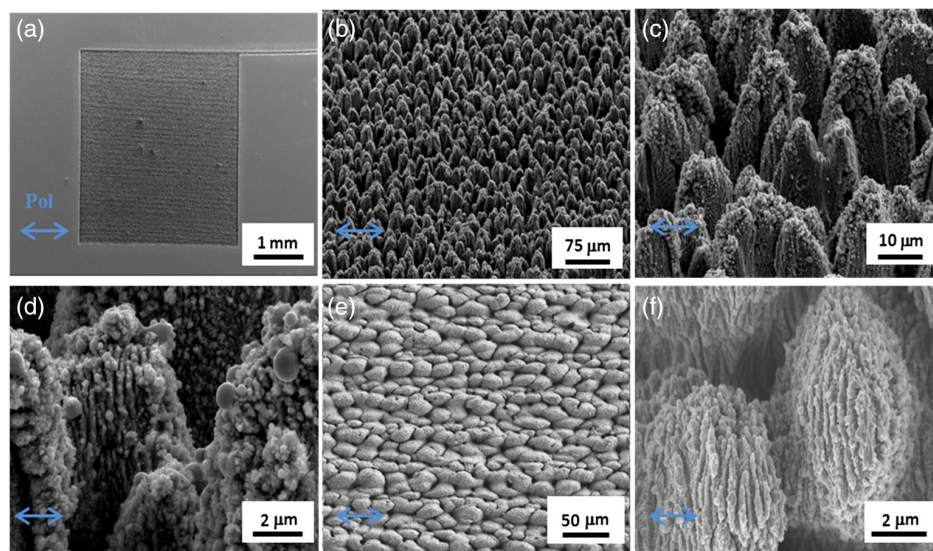


Figure 2. a) (0°), b–d) (60°) tilt-view SEM images of hierarchical spike structure produced by linearly polarized ablation of the Ti6Al4V surface with Ti:sapphire laser pulses ($\tau = 30 \text{ fs}$, $E = 70 \mu\text{J}$, repetition frequency = 1 kHz). e,f) Top-view SEM images of anodized + laser patterned surface structure. Blue arrow indicates the laser polarization direction.

cones are densely packed and possess a high aspect ratio. Such a high aspect ratio alone can result in superhydrophobicity.^[34] A high-resolution image (Figure 2d) reveals nanoripples superimposed on the spikes. This type of structure is produced due to unique interaction of a spatially Gaussian distributed laser beam with the surface of the metal. Formation of these structures by laser is still not thoroughly understood but it is supposed that the micrometric spikes are produced due to the presence of highly reflective impurities, i.e., inhomogeneous structure. Higher absorption intensity by electron–phonon interaction around this impurity causes ablation of the material, hence transforming the flat surface into cone or spike.^[35] In contrast, laser-induced periodic surface structures (LIPSS) are associated with the superposition of incident, refracted, reflected, and diffracted laser light near the interface causing periodic distribution of energy at the surface. This periodic distribution of energy results in the formation of periodic nanostructures.^[35]

Figure 2e–f shows the 0° tilt (top view) SEM images of fs laser-treated sample after anodization. It can be seen that the LIPSS structure is considerably more visible and the surface is comparatively brighter. The main reason is the formation of an additional oxide layer on the surface after anodization which can significantly fill up the nanopores on one hand, and influences the electrical properties of the surface on the other hand. A change in surface color shade from black to blackish brown was also experienced through the naked eye.

It is a well-known phenomenon that the oxide produced by the anodization does not only increase the wettability of the valve metal but also influences the surface chemistry.^[8] Keeping in mind the highly hydrophobic surface^[33] produced by fs laser ablation, it is important to know up to which content the surface is anodized. The electrochemically active surface area (ECSA) during anodization can be calculated by Faraday's law if the anodized oxide thickness is known. For this purpose, initially, 1 V stepwise increment cyclic voltammetry (CV) experiments were conducted on flat mechanically polished surfaces. By calculating the total charge ($\int I dt$), the resulting thickness (d_{ox}) was determined from Equation (1).

$$d_{\text{ox}} = \frac{MIt}{zF\rho_{\text{ox}}A_f} \quad (1)$$

In the formula, M is the molecular mass equivalent, z is the equivalent number of electrons, and ρ_{ox} is the equivalent oxide mass density. All these parameters were calculated by considering the mixed matter model. Finally, F is the Faraday constant and A_f is the area of the mechanically polished flat titanium alloy in contact with the electrolyte.

During each anodic sweep step, the current is initially negligible but as the applied potential surpasses the previously formed oxide potential, an abrupt increase in current density (i) can be observed (Figure 3a). This sudden increase in the current is due

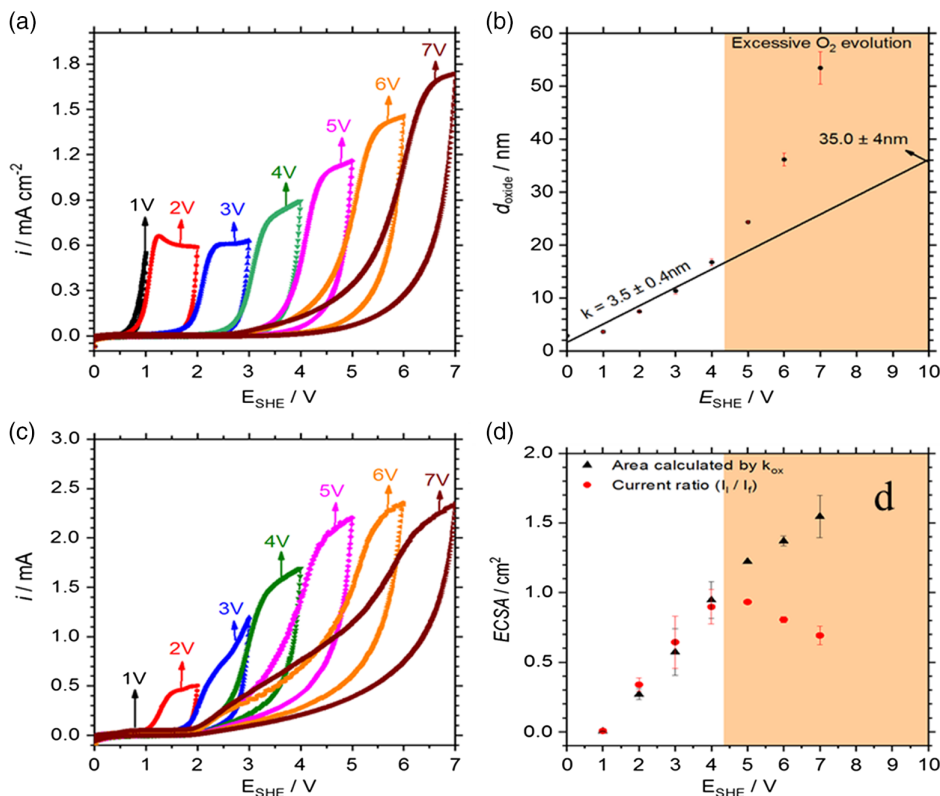


Figure 3. Cyclic voltammograms obtained by 1 V step increment in the voltage up to a maximum of a) 7 V for mirror polished surface and c) fs laser-treated Ti6Al4V alloy, respectively. b) Thickness estimation of anodized oxide layer formed on polished Ti6Al4V alloy surface after each increment in the voltage. d) Electrochemical surface area calculated using the Faraday's law for fs laser-treated sample by considering film formation factor k_{ox} (black color) and current ratio (I_i/I_r) (red).

to the combined movement of anions from electrolyte toward metal/oxide interface and cations from metal/oxide toward oxide/electrolyte interface. The energy for the anodization process is provided by the ion hopping mechanism initiated by the high field strength across the oxide film.^[25,26,36,37] In the absence of an electronic current (i.e., oxygen evolution and some semiconducting effects), the current should stabilize in the form of a current plateau after the steep current increase for potentiodynamic anodization process.^[36] However, due to excessive evolution of oxygen on TiO₂ for electric potentials above 4 V,^[13] the film thickness calculated by Faraday's law seems to be unrealistic. Thus, for the determination of film formation factor (k_{ox}), the slope of the first four thickness values were taken with respect to voltage step increment. A film formation factor of $3.5 \pm 0.4 \text{ nm V}^{-1}$ was evaluated and after extrapolating this slope to 10 V, a final anodic film thickness of $35 \pm 4 \text{ nm}$ was estimated. This value is in accordance with the highest value reported in the literature where light reflectance method was used to determine the thickness of anodized Ti6Al4V alloy at different voltages. A thickness of 38 nm was experimentally determined at an applied potential of 10 V.^[38] In contrast, much lower (k_{ox}) values were also found for Ti (2.5 nm V^{-1}) and Al (1.6 nm V^{-1}), respectively.^[25] The film formation factor value in this work can be slightly overestimated and the possible reasons can be dissolution of aluminum and vanadium in acidic electrolyte or higher k_{ox} number of vanadium (6.5 nm V^{-1}).^[38]

As the film formation factor is a material constant, it can be used to approximate the thickness of oxide grown on ECSA of fs laser-treated sample by means of Equation (2).

$$\text{Electrochemical surface area (ECSA)} = \frac{MIt}{zF\rho_{ox}k_{ox}V} \quad (2)$$

For this reason, once again a stepwise voltage increment was applied on fs laser-treated sample. In Figure 3c, it can be observed that the current transients are relatively different from

the flat samples. The cyclic voltammogram obtained at 1 V is unobservable most probably because the electrolyte is only in contact with the tips of the nanometer LIPSS structure and hence a negligible oxidation occurs. With the increase in anodization voltage, the electrolyte is progressively penetrating into the pores, thus causing an increase in electrolyte contact area. The main cause of this increment in the ECSA can be the electro-wetting phenomenon. The triple point between oxide, entrapped air in pores, and the electrolyte has a certain contact angle. This contact angle gets lower due to electrostatic interaction between electrolyte and oxide surface provided by voltage increment. The decrease in the contact angle ultimately can cause enhancement in the hydrophilic nature of oxide.^[39] Equation (2) was utilized to determine the ECSA while considering only the ionic contribution of the current transient and it is shown in Figure 3d that ECSA consistently increases as the applied voltage increases. Nevertheless, the oxygen evolution during anodization of titanium alloy is inevitable. It was observed during anodization that oxygen bubbles can stick to the surface, a fact which can affect the electrolyte contact area; thus, Equation (3) was also used for the calculation of ECSA.

$$\text{Electrochemical surface area (ECSA)} = \frac{I_l}{I_f} A_f \quad (3)$$

I_l and I_f are the total current produced during the anodization of fs laser-treated and flat mirror-like surface finished Ti6Al4V alloy samples, respectively. An optimum value of $0.968 \pm 0.08 \text{ cm}^2$ was found at 4 V which is approximately 8 times higher than the area of the flat sample (0.122 cm^2), as schematically shown in Figure 1b.

Figure 4a–b shows the superimposed Eh -pH diagrams of titanium, aluminum, and a separate diagram of vanadium at an activity of 10^{-6} M dissolved in 0.1 M H₂SO₄. The reason for choosing this activity was due to the continuous exposure of the new stream of electrolyte to the sample surface. A Pourbaix diagram

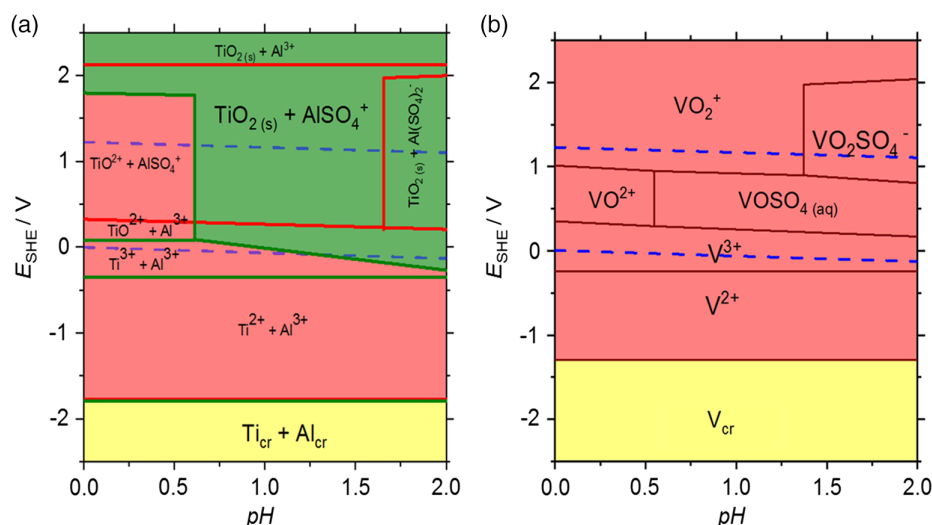


Figure 4. a) Simulated binary overlaid Pourbaix diagrams of Ti and Al at an activity of $a_{Ti} = a_{Al} = 10^{-6} \text{ mol L}^{-1}$ in 0.1 M H₂SO₄. b) Pourbaix diagram of vanadium ($a_V = 10^{-6} \text{ mol L}^{-1}$ in 0.1 M H₂SO₄). Light yellow-colored region in the diagram indicates the metallic or protected region, red and green regions point out the corrosion and passivity, respectively. Blue-colored lines specify the water oxidation (top) and reduction (below) window.

usually consists of three different types of lines. The vertical lines represent the electrochemical reactions which are only pH dependent (redox neutral transitions). The horizontal lines which solely represent the potential-dependent reactions (pH neutral transitions) and sloped lines explain the electrochemical reactions reliant on both pH and potential.^[40] The pH of 0.1 M H₂SO₄ was in the range of 0.7–1.0; therefore, the pH range of 0–2 is of interest. It is worth noting that in the simulated Pourbaix diagrams, aluminum and vanadium are corroding in this pH range above their redox potential, whereas titanium passivates due to the formation of TiO₂ in a wide range of pH (shown by the green region in Figure 4a). The stability of ionic species or a compound in standard condition depends upon the Gibbs free energy of its formation. Thermodynamically the more negative the Gibbs free energy is, the more stable the ion or compound is considered. **Table 1** shows the thermodynamic data calculated by equilibrium constant value for each reaction and ionic species. When a positive potential is applied to a metal, it loses the electrons depending upon the redox potential and electron affinity, i.e., Ti⁴⁺, V⁵⁺, Al³⁺. In the presence of oxygen and aqueous medium, the ion can either form an oxide (TiO₂), hydroxide, or it can dissolve into electrolyte in its solvated ionic state (Al·(H₂O)_x³⁺, AlSO₄·(H₂O)_x⁺, VO₂⁺, and so on). It is important to note that the Pourbaix diagram is only a map of possibilities depending upon thermodynamics. No information is provided for the rate of a reaction or kinetics.

Normally, the electrochemical reaction does not happen at standard conditions and in the potentiodynamic anodization processes, certain parameters, i.e., change in temperature, concentration of dissolved ions, scan rate, and rate-determining step in a reaction can play a handful role on the resulting product. To obtain further insight and compare the surface composition of substrate, laser-treated, and laser-treated + anodized Ti6Al4V alloy, XPS analysis was performed. **Figure 5a–c** shows the high-resolution XPS spectra of Al2p, V2p, and Ti2p. The qualitative analysis of Ti2p_{3/2} and Al2p_{3/2} shows that the maximum of both peaks is centered at a binding energy of

458.59 ± 0.07 and 73.9 ± 0.4 eV, respectively. These binding energy values are accordingly referred to TiO₂ and Al₂O₃ in the literature.^[41]

Furthermore, the quantitative analysis in relative weight percentage is given in the form of statistical distribution in Figure 5d. The relative weight percentage of titanium increased from 53.7 to 62.5 wt%, aluminum demonstrates a decline from 42.9 to 34.3 wt%, and vanadium exhibited relatively very small change from 3.4 to 3.2 wt% after fs laser treatment. As the evaporation temperature of aluminum (2327 °C) is considerably lower than vanadium (3407 °C) and titanium (3287 °C), it is possible that aluminum was preferentially ablated at a higher rate compared with titanium and vanadium.

The XPS analysis on the laser-treated + anodized sample revealed that titanium increases again from 62.5 to 72.8 wt%, which can be due to the passivation of titanium during anodization as explained earlier in the Pourbaix diagram section. Similarly, aluminum shows a decrease from 34.3 to 23.8 wt% after anodization, which can be related to the dissolution of aluminum in the form of Al(SO₄)₂⁻ or AlSO₄⁺ as both of them have lowest free energy formation of -1998.80 and -1225.6 kJ mol⁻¹, respectively. However, due to the strong affinity of aluminum and titanium toward oxygen, it is likely that Al and Ti react with oxygen and water to produce Al₂O₃ (ΔG_r = -1574.9 kJ mol⁻¹) and TiO₂ which is quite evident from the binding energies of Al2p_{3/2} and Ti2p_{3/2} in the XPS curves. The reason of lower change in relative weight percentage of vanadium even after anodization can be as follow: 1) lower affinity toward oxygen and higher oxidation potential of V compared with Al and Ti; 2) lower transportation number of V (0.28)^[42] compared with Al (0.5) and Ti (0.35) during anodization.

Considering these two points, it can be inferred that Al and Ti grow oxides much more effectively and can incorporate vanadium inside the oxide layer leaving less vanadium exposed to electrolyte for further dissolution.

Previous study on the used leadless heart pacemakers revealed that the surface of these devices are overgrown by fibroblast cells

Table 1. Standard Gibbs free energy of formation for each species and also for each reaction indicated in Pourbaix diagram.

Chemical reactions	ΔG _r ^o [kJ mol ⁻¹]	ln K _c	Species	ΔG _f ^o [kJ mol ⁻¹]
2H ₂ O = 4 H ⁺ + O ₂ + 4e ⁻	474.27		H ₂ O, H ⁺ , e ⁻	-237.37, 0, 0
Al ³⁺ + 3e ⁻ = Al _(cr)	481.02	-194.14	Al ³⁺	-481.01
Al ³⁺ + SO ₄ ²⁻ = AlSO ₄ ⁺	-19.97	8.061	AlSO ₄ ⁺	-1225.6
Al ³⁺ + 2SO ₄ ²⁻ = Al(SO ₄) ₂ ⁻	28.543	11.52	Al(SO ₄) ₂ ⁻	-1998.8
Ti ³⁺ + 3e ⁻ = Ti _(cr)	349.829	-141.19	Ti ³⁺	-349.829
Ti ³⁺ + e ⁻ = Ti ²⁺	35.654	-14.39	Ti ²⁺	-314.17
Ti ³⁺ + H ₂ O = 2 H ⁺ + e ⁻ + TiO ²⁺	9.638	-3.89	TiO ²⁺	-577.561
Ti ³⁺ + 2H ₂ O = 4 H ⁺ + e ⁻ + TiO _{2(s)}	-17.745	7.162	TiO _{2(s)}	-841.84
V ²⁺ + 2e ⁻ = V _(cr)	217.975	-87.974	V ²⁺	-217.975
V ²⁺ = V ³⁺ + e ⁻	-24.591	9.925	V ³⁺	-242.566
V ²⁺ + H ₂ O = 2 H ⁺ + 2e ⁻ + VO ²⁺	7.929	-3.2	VO ²⁺	-447.41
V ²⁺ + SO ₄ ²⁻ + H ₂ O = 2 H ⁺ + 2e ⁻ + VOSO _{4(aq)}	-6.046	2.44	VOSO _{4(aq)}	-1206.02
V ²⁺ + SO ₄ ²⁻ + 2H ₂ O = 4 H ⁺ + 2e ⁻ + VO ₂ SO ₄ ⁻	-94.778	38.252	VO ₂ SO ₄ ⁻	-1531.64
V ²⁺ + 2H ₂ O = 4 H ⁺ + 3e ⁻ + VO ₂ ⁺	104.535	-42.19	VO ₂ ⁺	-796.78

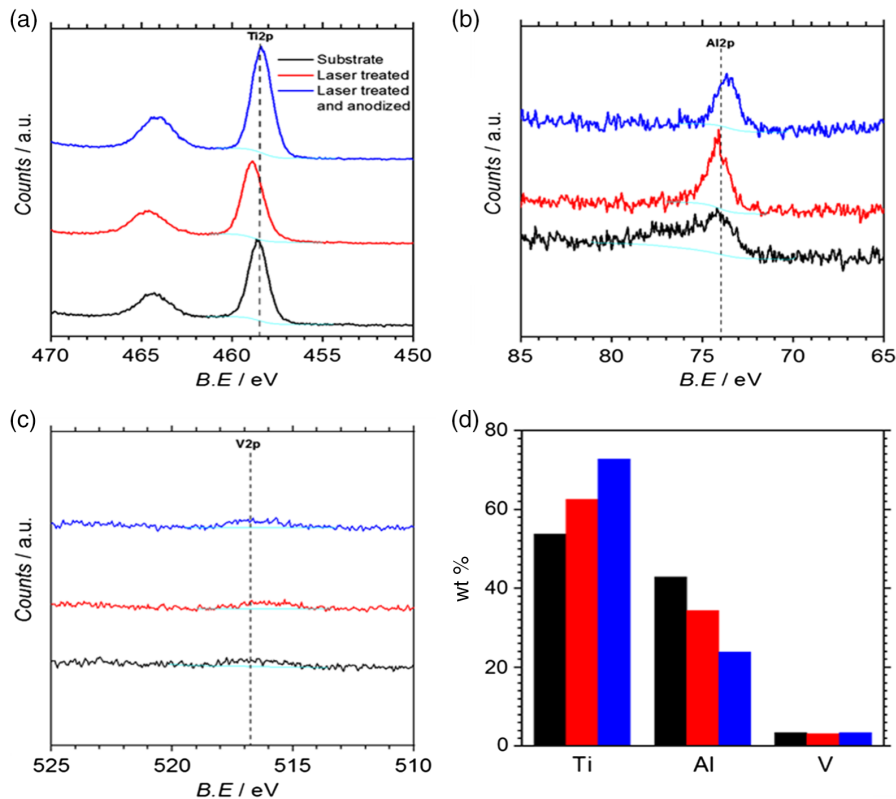


Figure 5. High-resolution XPS scans for a) Ti2p, b) V2p, c) Al2p, and d) statistical comparison of weight percentage of titanium, aluminum, and vanadium before and after each surface treatment process.

or the collagens produced by these cells.^[7] That is why, in the current work, cell adhesion experiments were undertaken in the murine fibroblast cell environment. Fibroblast cell adhesion on the implant surface is mainly governed by the focal adhesive sites. These sites are the locations where the distance between cell membrane and implant surface is less than 10–15 nm.^[43] In case of flat titanium surface, these sites are considerably higher in number and result in better cell proliferation.

Similar justification can be given for the flat anodized Ti alloy sample shown in **Figure 6a,b** (left to the dotted line) where cells are grown in the form of multilayered and elongated shape (common for fibroblasts). These cells are densely packed and are exhibiting a nonpreferred directional growth.

On the contrary, fibroblast cells grown on fs laser-treated + anodized surface shown in **Figure 6a,b** (right to the dotted line) are mostly round in shape occasionally elongated and sometimes

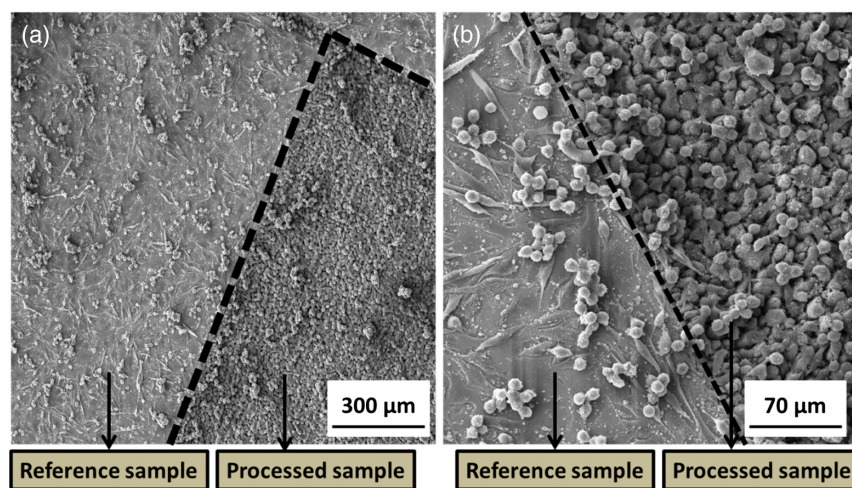


Figure 6. a,b) SEM images of flat anodized reference Ti6Al4V alloy overgrown by the murine fibroblast cells (left side of the dotted line in both images) and fs laser + anodized Ti6Al4V alloy surface (right side of the dotted line) after an exposure time of ≈ 1 week in murine fibroblast cell environment.

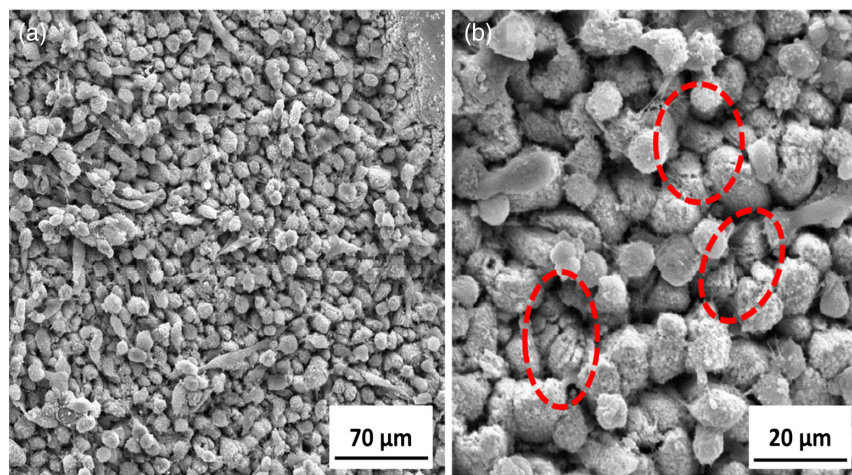


Figure 7. a) SEM image of Ti alloy surface with Ti:sapphire laser-induced spikes combined with anodization at 10 V versus SHE a) after 1 week of seeding time in fibroblast cell culture medium and b) magnified image of the similar surface, whereas dotted red circular areas show the cell-free spike surfaces.

forming small clusters. These round-shaped cells are nonadherent to each other and conical spike texture produced by fs laser treatment in a preferred orientation can still be perceived easily in Figure 6a.

Further examination of high-resolution SEM images in Figure 7a–b demonstrates that the surface is not completely covered with fibroblast cells. There are some areas where LIPSS structures are completely exposed shown by dotted red circles. This clearly indicates that cell growth is restricted due to some repulsive behavior provided by special surface texture. The repulsive behavior of these cells can be explained as follow: 1) According to Ponsonnet et al.,^[44] the cell proliferation decreases drastically as the average peak to valley distance of surface protrusion on Ti alloy is over a threshold limit of (0.08–1 μm). In this work, conical or spike-like structures with superimposed nanostructure LIPSS were produced by fs laser ablation carrying an approximate tip-to-tip distance of more than 2 μm and peak-to-valley distance of greater than ≈10 μm; thus, it is possible that cells are only attached to the tip of these spikes and due to lower aerial contact area, the cells cannot follow the sharp periodic texture. 2) Extracellular matrix and proteins are important to create an adsorbed layer for the attachment of the cells to the implant surface.^[14] Depending on the volume of these proteins, it is possible that some of them cannot accommodate within the nanostructures produced by laser treatment. This size indifference can also be the possible reason of reluctant growth behavior of fibroblast cells on titanium alloy. 3) Spike formed on the flat surface can cause isolation and bending of the cell. This cell bending can ultimately cause disruption of cytoskeleton and thus it becomes difficult to grow and connect the cells together.^[43]

4. Conclusions

Through fs laser treatment, a hierarchical surface structure composed of micrometer spikes and superimposed nanoripple-like structures was successfully produced on a Ti6Al4V alloy surface. Anodization was performed on these samples and it was found

that the electrochemical surface area is approximately 8 times larger than the flat titanium alloy sample. Finally, cell growth experiments revealed that the combined fs laser treatment and anodization can be used to produce fibroblast cell-free implant surfaces.

Acknowledgements

The authors acknowledge the CellFreeImplant project funded by the European Union Horizon 2020 research and innovation program under grant agreement number 800832. The financial support by the Austrian Federal Ministry of Science, Research and Economy and the National Foundation for Research, Technology and Development through the Christian Doppler Laboratory for Combinatorial Oxide is gratefully acknowledged. The financial support received from the European Union Horizon 2020 through the project Medical Device Obligation Taskforce (MDOT) is gratefully acknowledged. MDOT received funding from the European Union's Horizon 2020 research and innovation program under grant agreement number 814654. The authors would like to thank S. Benemann (BAM 6.1) for SEM characterization and S. Binkowski (BAM 6.3) for polishing the titanium samples.

Conflict of Interest

The authors declare no conflict of interest.

Keywords

anodization, femtosecond laser ablation, laser-induced periodic surface structures, Ti6Al4V alloys, X-ray photoelectron spectroscopy

Received: October 3, 2019
Revised: January 15, 2020
Published online: June 17, 2020

- [1] J. C. Schuster, M. Palm, *J. Phase Equilib. Diffus.* **2006**, 27, 3.
[2] J. R. Davis, *Alloying: Understanding the Basics*, ASM International, Cleveland, OH **2001**.

- [3] A. I. Mardare, A. Savan, A. Ludwig, A. D. Wieck, A. W. Hassel, *Electrochim. Acta* **2009**, *54*, 5973.
- [4] P. Bleckenwegner, C. C. Mardare, C. Cobet, J. P. Kollender, A. W. Hassel, A. I. Mardare, *ACS Comb. Sci.* **2017**, *19*, 121.
- [5] İ. Merve, B. Ercan, *Chem. Sci. Eng.* **2019**, *13*, 28.
- [6] K. Prasad, O. Bazaka, M. Chua, M. Rochford, L. Fedrick, J. Spoor, R. Symes, M. Tieppo, C. Collins, A. Cao, D. Markwell, K. Ostrikov, K. Bazaka, *Materials* **2017**, *10*, 884.
- [7] A. Kypa, H. Blessberger, J. Kammler, M. Lichtenauer, T. Lambert, R. Silye, C. Steinwender., *Can. J. Cardiol.* **2016**, *32*, 12.
- [8] M. Kulkarni, A. Mazare, E. Gongadze, Š. Perutkova, V. Kralj-Iglič, I. Milošev, P. Schmuki, A. Iglič, M. Mozetič, *Nanotechnology* **2015**, *26*, 062002.
- [9] Y. Okazaki, Y. Ito, K. Kyo, T. Tateishi, *Mater. Sci. Eng. A* **1996**, *213*, 138.
- [10] H. Song, M. Kim, G. Jung, M. Vang, Y. Park, *Surf. Coat. Tech.* **2007**, *201*, 8738.
- [11] J. P. Kollender, A. I. Mardare, A. W. Hassel, *J. Electrochem. Soc.* **2017**, *164*, c598.
- [12] J. P. Kollender, C. C. Mardare, A. I. Mardare, A. W. Hassel, *J. Solid State Electrochem.* **2018**, *22*, 2457.
- [13] J. P. Kollender, A. W. Hassel, *ChemElectroChem* **2017**, *4*, 1846.
- [14] L. Richert, F. Variola, F. Rosei, J. D. Wuest, A. Nanci, *Surf. Sci.* **2010**, *604*, 1445.
- [15] C. Y. Guo, J. P. Matinlinna, A. Tin, H. Tang, *Int. J. Biomater.* **2012**, *2012*, 381535.
- [16] F. Rupp, R. A. Gittens, L. Scheideler, A. Marmur, B. D. Boyan, Z. Schwartz, J. Geis-Gerstorfer, *Acta Biomater.* **2014**, *10*, 2894.
- [17] C. N. Elias, C. Nelson, F. Rocha, A. Lucia, P. Guilherme, *J. Mech. Behav. Biomed. Mater.* **2012**, *16*, 169.
- [18] M. E. Yurttutan, A. Keskin, *BMC Oral Health* **2018**, *18*, 47.
- [19] D. V. Portan, F. Nikolopoulou, V. Bairami, D. Mouzakis, G. C. Papanicolaou, D. D. Deligianni, *J. Mater. Sci. Surf. Eng.* **2016**, *4*, 376.
- [20] F. Cristiano, *Ion Implantation-Induced Extended Defects: Structural Investigations and Impact on Ultra-Shallow Junction Properties, Habilitation Treatise*, Université Paul Sabatier – Toulouse III, Toulouse, France **2013**.
- [21] B. Moore, E. Asadi, G. Lewis, *Adv. Mater. Sci. Eng.* **2017**, *2017*, 5812907.
- [22] X. Wang, C. Li, C. Ma, J. Feng, W. Hong, Z. Zhang, *Opt. Express* **2018**, *26*, 6325.
- [23] F. A. Müller, C. Kunz, S. Gräf, *Materials* **2016**, *9*, 476.
- [24] X. Shen, P. Ma, Y. Hu, G. Xu, J. Zhou, K. Cai, *Colloid. Surface B* **2015**, *127*, 221.
- [25] A. W. Hassel, D. Diesing, *Thin Solid Films* **2002**, *414*, 296.
- [26] A. I. Mardare, A. Savan, A. Ludwig, A. D. Wieck, A. W. Hassel, *Corros. Sci.* **2009**, *51*, 1519.
- [27] M. Sarraf, E. Zalnezhad, A. R. Bushroa, A. M. S. Hamouda, A. R. Rafieerad, B. Tabrizi, *Ceram. Int.* **2015**, *41*, 7952.
- [28] J. P. Kollender, M. Voith, S. Schneiderbauer, A. I. Mardare, A. W. Hassel, *J. Electroanal. Chem.* **2015**, *740*, 53.
- [29] A. I. Mardare, A. W. Hassel, *Rev. Sci. Instrum.* **2009**, *80*, 046106.
- [30] A. W. Hassel, D. Diesing, *Electrochem. Commun.* **2002**, *4*, 1.
- [31] A. W. Hassel, D. Diesing, *J. Electrochem. Soc.* **2007**, *154*, C558.
- [32] I. Puigdomenech, Department of Inorganic Chemistry, Royal institute of Technology, Stockholm, Sweden **2010**, <http://www.kemi.kth.se/medusa>.
- [33] J. Heitz, C. Plamadela, M. Muck, O. Armbruster, W. Baumgartner, A. Weth, C. Steinwender, H. Blessberger, J. Kellermair, S. V. Kirner, J. Krüger, J. Bonse, A. S. Guntner, A. W. Hassel, *Appl. Phys. A Mater.* **2017**, *123*, 734.
- [34] A. W. Hassel, S. Milenkovic, U. Schürmann, H. Greve, V. Zaporojtchenko, R. Adelung, F. Faupel, *Langmuir* **2007**, *23*, 2091.
- [35] D. Bäuerle, *Laser Processing and Chemistry*, Springer, Heidelberg, Germany, **2011**.
- [36] A. I. Mardare, *High Throughput Growth of Anodic Oxides on Valve Metals: Combinatorial Thin Film Material Libraries – Growth, Modification and Characterization of Anodic Oxides*, VDM Verlag Dr. Müller, Germany, **2010**.
- [37] M. M. Lohrengel, *Mater. Sci. Eng. R* **1993**, *11*, 243.
- [38] A. Karambakhsh, A. Afshar, P. Malekinejad, *J. Mater. Eng. Perform.* **2012**, *21*, 121.
- [39] Y. Zhao, Y. Wang, *Rev. Adhes. Adhes.* **2013**, *1*, 114.
- [40] M. Pourbaix, *Corros. Sci.* **1990**, *30*, 963.
- [41] C. D. Wagner, *The NIST X-Ray Photoelectron Spectroscopy Database*, NIST, Washington, DC, **1991**.
- [42] W. D. Mackintosh, H. H. Plattner, *J. Electrochem. Soc.* **1976**, *123*, 523.
- [43] L. Ponsonnet, M. Lissac, N. Jaffrezic, V. Comte, C. Lagneau, M. Lissac, C. Martelet, M. Charbonnier, *Mater. Sci. Eng. C* **2002**, *21*, 157.
- [44] L. Ponsonnet, K. Reybier, N. Jaffrezic, V. Comte, C. Lagneau, M. Lissac, C. Martelet, *Mater. Sci. Eng. C* **2003**, *23*, 551.